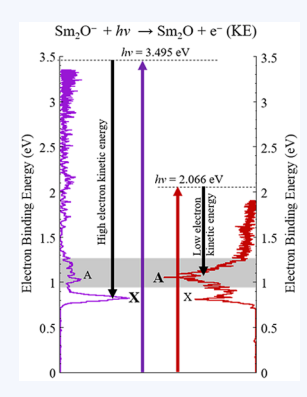


# **Exceptionally Complex Electronic Structures of Lanthanide Oxides** and Small Molecules

Jarrett L. Mason, † Hassan Harb, † Josey E. Topolski, † Hrant P. Hratchian, \*\*, † 100 and Caroline Chick Jarrold\*,†

CONSPECTUS: Lanthanide (Ln) oxide clusters and molecular systems provide a bottom-up look at the electronic structures of the bulk materials because of close parallels in the patterns of Ln 4f<sup>N</sup> subshell occupancy between the molecular and bulk Ln<sub>2</sub>O<sub>3</sub> size limits. At the same time, these clusters and molecules offer a challenge to the theory community to find appropriate and robust treatments for the 4f<sup>N</sup> patterns across the Ln series. Anion photoelectron (PE) spectroscopy provides a powerful experimental tool for studying these systems, mapping the energies of the ground and low-lying excited states of the neutral relative to the initial anion state, providing spectroscopic patterns that reflect the Ln 4f<sup>N</sup> occupancy. In this Account, we review our anion PE spectroscopic and computational studies on a range of small lanthanide molecules and cluster species. The PE spectra of  $LnO^-$  (Ln = Ce, Pr, Sm, Eu) diatomic molecules show spectroscopic signatures associated with detachment of an electron from what can be described as a diffuse Ln 6s-like orbital. While the spectra of all four diatomics share this common transition, the fine structure in the transition becomes more complex with increasing 4f occupancy. This



effect reflects increased coupling between the electrons occupying the corelike 4f and diffuse 6s orbitals with increasing N. Understanding the PE spectra of these diatomics sets the stage for interpreting the spectra of polyatomic molecular and cluster species.

In general, the results confirm that the partial 4f<sup>N</sup> subshell occupancy is largely preserved between molecular and bulk oxides and borides. However, they also suggest that surfaces and edges of bulk materials may support a low-energy, diffuse Ln 6s band, in contrast to bulk interiors, in which the 6s band is destabilized relative to the 5d band. We also identify cases in which the molecular Ln centers have  $4f^{N+1}$  occupancy rather than bulklike  $4f^N$ , which results in weaker Ln—O bonding. Specifically, Sm centers in mixed Ce-Sm oxides or in  $Sm_xO_y^-$  ( $y \le x$ ) clusters have this higher  $4f^{N+1}$  occupancy. The PE spectra of these particular species exhibit a striking increase in the relative intensities of excited-state transitions with decreasing photon energy (resulting in lower photoelectron kinetic energy). This is opposite of what is expected on the basis of the threshold laws that govern photodetachment. We relate this phenomenon to strong electron-neutral interactions unique to these complex electronic structures. The time scale of the interaction, which shakes up the electronic configuration of the neutral, increases with decreasing electron momentum.

From a computational standpoint, we point out that special care must be taken when considering Ln cluster and molecular systems toward the center of the Ln series (e.g., Sm, Eu), where treatment of electrons explicitly or using an effective core potential can yield conflicting results on competing subshell occupancies. However, despite the complex electronic structures associated with partially filled 4f<sup>N</sup> subshells, we demonstrate that inexpensive and tractable calculations yield useful qualitative insight into the general electronic structural features.

3265

# 1. INTRODUCTION

Lanthanides (Ln), customarily relegated to the bottom margin of the periodic table of the elements with the actinides, are a series of elements whose atomic electronic structures are characterized by close-lying 6s, 5d, and 4f subshells, ranging from lanthanum (4f<sup>0</sup>5d6s<sup>2</sup>) to ytterbium (4f<sup>14</sup>6s<sup>2</sup>). Ln<sub>2</sub>O<sub>3</sub> bulk properties are similar: Ln 4f occupancy tends to increase incrementally with atomic number. Electrons in the corelike 4f subshell are nuclear-shielding, and  $Z_{\rm eff}$  is consequently relatively constant, resulting in very similar chemical properties for near-neighbors in this row. The 4f subshell occupancy of the Ln ion in lanthanide oxides (generally  $Ln_2O_3$ ) is generally the same as in the atom.<sup>2</sup>

Cerium is the lightest *Ln* atom with 4f subshell (single) occupancy, and despite the "rare earth" moniker, it is more abundant in the earth's crust than both copper and nickel.<sup>3</sup> Intrigued by the burst of interest in ceria as a catalyst support material, 4,5 we undertook several cerium oxide cluster anion reactivity studies<sup>6-8</sup> and determined the molecular and electronic structures of these clusters by anion photoelectron

Received: September 6, 2019 Published: November 8, 2019

Department of Chemistry, Indiana University, 800 East Kirkwood Avenue, Bloomington, Indiana 47405, United States

<sup>&</sup>lt;sup>‡</sup>Department of Chemistry and Chemical Biology and Center for Chemical Computation and Theory, University of California, Merced, 5200 North Lake Road, Merced, California 95343, United States

(PE) spectroscopy and density functional theory (DFT) studies. However, to better understand the complex electronic structures arising in systems with partially filled 4f subshells, we investigated a number of  $LnO/LnO^-$  diatomics  $^{10-13}$  and small mono-Ln polyatomics. These studies informed subsequent analyses of studies on mixed metal oxide clusters,  $^{12,17,18}$  some of which exhibited new and anomalous features in their anion PE spectra.  $^{19,20}$ 

To set the stage, we invoke a useful construct used by Field in a seminal paper detailing the ligand field theory treatment of *LnO* electronic structure, <sup>21</sup> the "superconfiguration," which is a simplified, general characterization of the orbital occupancy shared by the constellation of close-lying electronic states in these systems. For example, the Ce<sup>2+</sup> center in the ground state of the CeO molecule, the subject of numerous detailed spectroscopic<sup>22–25</sup> and ab initio<sup>26,27</sup> investigations, has a singly occupied 4f orbital and a singly occupied diffuse 6s-like orbital: its superconfiguration is 4f6s. More highly oxidized lanthanide centers may have empty 4f and 6s subshells.<sup>14,28,29</sup>

Why do so many close-lying electronic states arise from the 4f6s superconfiguration? We first consider the spin-orbit coupling in Ce<sup>2+</sup> with the 4f6s superconfiguration. Ce is a fairly heavy element, with strong spin-orbit coupling, and the j-jcoupling scheme, where the angular momenta of the individual electrons are considered separately  $(j_{b}, j_{s})$  and then combined to obtain the total electron angular momentum (Ja for the atomic center), is appropriate. In the j-j coupling scheme, the  $Ce^{2+}$  center has lower-energy states with  $J_a = 2$  or 3 from  $j_f =$  $^{5}/_{2}$  (4f electron) and  $j_{s} = \pm^{1}/_{2}$  (6s electron) that are very closelying, along with higher-energy states with  $J_a = 4$  or 3 from  $j_f =$  $\sqrt{2}/2$ ,  $j_s = \pm \sqrt{1}/2$ . The electrons in the 4f and 6s orbitals are very weakly coupled. These relative energies are largely preserved in the ligand field of O2-, leading to 16 close-lying states associated with projections of  $J_a$  onto the internuclear axis,  $\Omega$ . The case is somewhat simpler for the seven electronic states of CeO<sup>-</sup> with the 4f6s<sup>2</sup> superconfiguration, resulting in  $J_a = \frac{5}{2}$ and the higher-lying  $J_a = \frac{7}{2}$  states.<sup>10</sup> The anion states and (known) neutral states are shown schematically in Figure 1.<sup>23</sup>

# 2. ELECTRONIC STRUCTURES OF *Ln*O DIATOMIC ANIONS AND NEUTRALS

Considering the electronic states summarized in Figure 1, the PE spectrum of CeO<sup>-</sup> should reflect detachment transitions involving the 6s orbital, i.e., CeO<sup>-</sup>[4f6s] + e<sup>-</sup>(KE)  $\leftarrow$  CeO<sup>-</sup>[4f6s²]. Despite the energetic proximity of the 4f and 6s orbitals, the 4f<sup>0</sup>6s² superconfiguration lies much higher in energy. In addition, one of our previous findings from measuring the spectrum of Ce<sup>-</sup> is that the cross section for detaching an electron from a 4f orbital is comparatively very small, <sup>30</sup> as predicted theoretically. <sup>31</sup> Assuming that one-electron transitions are dominant, we expect a change *only* in  $j_s$  ( $\Delta j_s = -\frac{1}{2}$ ,  $+\frac{1}{2}$ ), with  $j_f$  being conserved (as illustrated in Figure 1). From the lowest-lying state of the anion, only the two lowest-lying neutral states are accessible. However, the assumption of one-electron transitions may not be appropriate (vide infra). <sup>32</sup>

Figure 2 shows the PE spectra of CeO<sup>-</sup>, PrO<sup>-</sup>, SmO<sup>-</sup>, and EuO<sup>-</sup> (contributions from the EuOH<sup>-</sup> contaminant are shown as orange peaks) measured using an experimental apparatus described previously.<sup>33,34</sup> Spectra measured with the laser polarization parallel and perpendicular to the electron drift path are both shown: the spectra measured with parallel

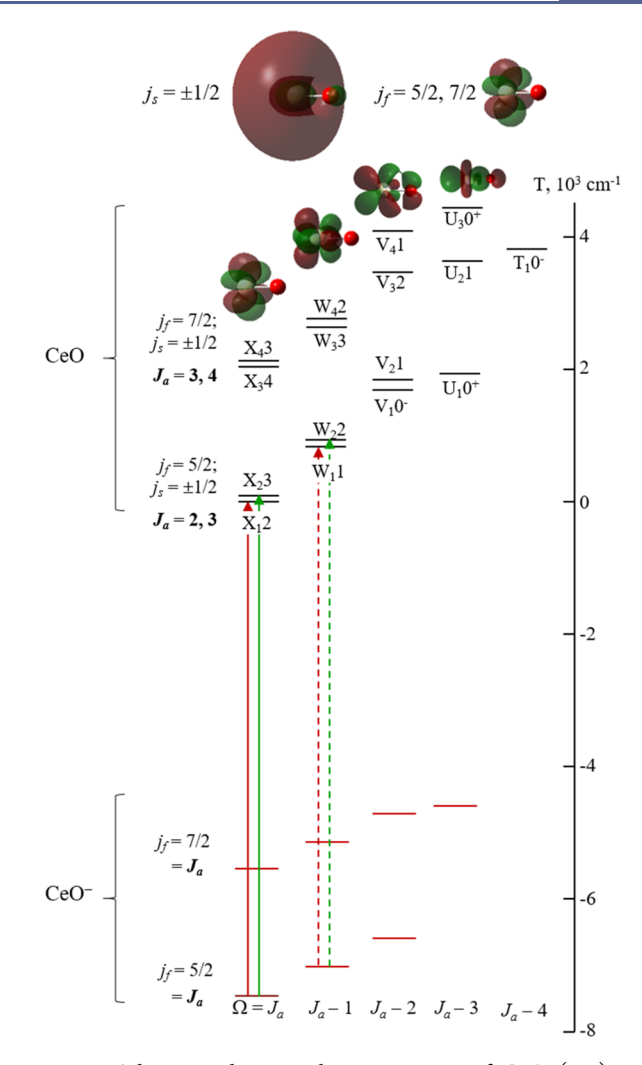


**Figure 1.** Schematic showing electronic states of CeO (top) and CeO<sup>-</sup> (bottom) resulting from the 4f6s and 4f6s<sup>2</sup> superconfigurations, respectively. One-electron-allowed transitions from the two lowest-energy states of the anion are indicated with arrows, with red indicating the transition to the lowest-energy one-electron-accessible state of the neutral  $(\Delta j_s = -^1/_2)$  and green indicating the close-lying but higher-energy transition  $(\Delta j_s = +^1/_2)$ . Energies and labels for the CeO neutral states were adapted from ref 23.

polarization are more intense than those with perpendicular polarization, which is consistent with detachment from the 6s orbital. <sup>35,36</sup> An obvious trend in these spectra is increasing spectral congestion with increasing 4f subshell occupancy. The spectrum of CeO<sup>-</sup> is very simple and appears to be a single transition with a short vibrational progression, though in fact two electronic transitions separated by 84 cm<sup>-1</sup> are present (Figure 1). The PE spectrum of PrO<sup>-</sup> supports this assertion: the splitting between the analogous  $\Delta j_s = -\frac{1}{2}, +\frac{1}{2}$  transitions in PrO<sup>-</sup> is slightly larger, and the two transitions are partially resolved in the spectrum (Figure 2b).

The spectrum of SmO¯ exhibits numerous overlapping transitions, as confirmed by higher-resolution slow photo-electron velocity-map imaging of cryo-cooled anions (cryo-SEVI) measurements by Neumark and co-workers, <sup>32</sup> reflecting extensive mixing between close-lying neutral states arising from the 4f 6s superconfiguration. This observation is a distinct indication that the one-electron view of photodetachment transitions is inadequate. Indeed, the low-intensity transitions

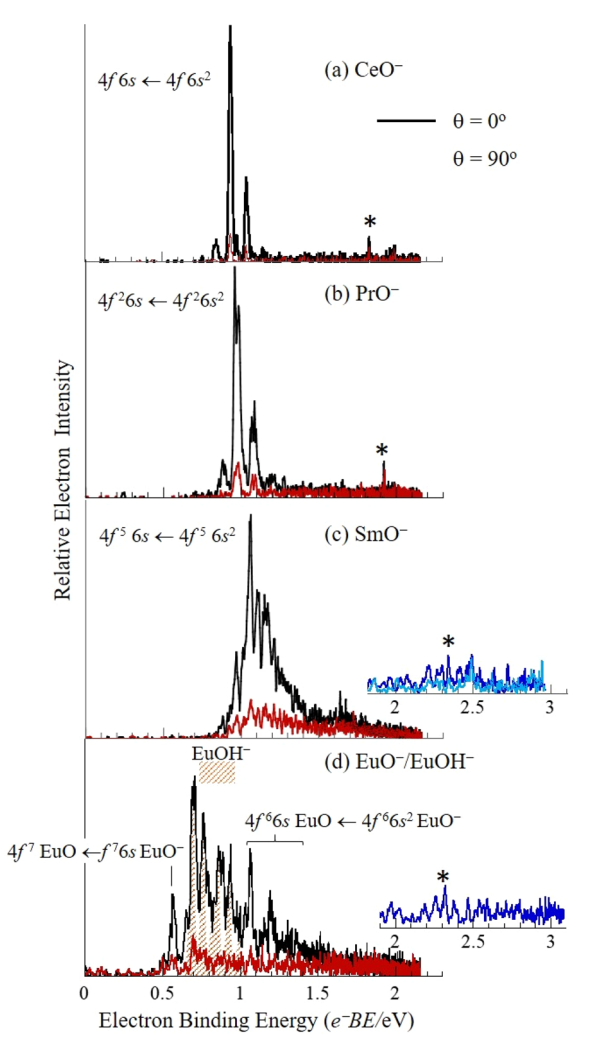


**Figure 2.** Anion PE spectra of (a) CeO<sup>-</sup> ( $4f6s^2$  superconfiguration), (b) PrO<sup>-</sup> ( $4f^26s^2$ ), (c) SmO<sup>-</sup> ( $4f^66s^2$ ), and (d) overlapping EuO<sup>-</sup> ( $4f^66s^2$ ) and  $4f^66s^2$ ) and EuOH<sup>-</sup>. All exhibit analogous  $LnO(4f^N6s) + e^-(KE) \leftarrow LnO^-(4f^N6s^2)$  transitions, with additional transitions evident in (d). As N increases, spectral congestion increases because of increased coupling between electrons in the corelike 4f and diffuse 6s orbitals. The spectra were measured with a photon energy of 2.330 eV (532 nm) with the laser polarization parallel to (black) or perpendicular to (red) the electron drift path. Portions of the PE spectra of SmO<sup>-</sup> and EuO<sup>-</sup>/EuOH<sup>-</sup> measured with a photon energy of 3.495 eV (355 nm) are included as blue traces to show the low-intensity signals assigned to transitions involving two electrons (detachment and excitation), indicated with an asterisk (\*) at higher electron binding energy for all four species.

indicated by asterisks (\*) in Figure 2 are at energies where no one-electron transitions are predicted, though ab initio calculations on low-lying excited states of CeO predict  $6s \rightarrow 5d$  transitions to states that lie approximately 1.25 eV above the ground state.<sup>37</sup> We had suggested that these low-intensity features are shake-up (two-electron) transitions  $^{10-13}$  in which detachment of an electron from the doubly occupied 6s orbital is accompanied by a  $6s \rightarrow 5d_{\pi}$  promotion of the other electron. Shake-up transitions are not without precedent, having been observed previously in anion PE spectra.  $^{38}$  Curiously, theoretical calculations attending the cryo-SEVI study of SmO<sup>-</sup> did not predict states in the energy range of the observed (\*) transitions;  $^{32}$  nonetheless, the fact that they were observed is a reflection of how fraught calculations on complex

molecules like SmO can be and how critical experimental measurements are for characterizing these species. We note that these (\*) transitions are not due to detachment of electrons from 4f orbitals, which as noted previously have exceptionally small photodetachment cross sections, in contrast to the exceptionally large cross sections for transitions associated with 6s electron detachment. <sup>14,30,31</sup>

In our studies on these small molecules, DFT calculations provided useful qualitative results. Good agreement between the relative energies of the anions and neutrals along with the range of neutral energies from a particular superconfiguration was achieved using the B3LYP hybrid density functional with an effective core potential (ECP) employed to implicitly treat scalar relativistic effects. However, in the case of EuO, for which the  $4f^7$  and  $4f^6$ 6s superconfigurations are competitive, use of an ECP and an all-electron basis set with explicit inclusion of scalar relativistic effects gave conflicting results as to which is lower in energy. Calculations on mid-lanthanoids must therefore be treated with caution and care.

Since the goal of the studies summarized in this section was to gain insight into the electronic structures of more complex molecules and clusters, a summary of these insights is warranted and follows:

- (i) Anion and neutral diatomics generally shared the same 4f subshell occupancies, with excess charge in the anion carried in a diffuse nonbonding *Ln* 6s orbital.
- (ii) Large photodetachment cross sections and parallel transitions are hallmarks of a detachment transition associated with the 6s orbital. These electrons are not strongly bound.
- (iii) With initial 4f°6s² superconfigurations, shake-up transitions that appear to involve promotion of a 6s electron to a 5d (or possibly 6p) orbital coupled with detachment of an electron from the 6s orbital appear to be a common phenomenon.
- (iv) With increasing 4f subshell occupancy, increased mixing between the states within the manifold associated with a particular superconfiguration results in greater spectral congestion, pointing to the inadequacy of treating transitions as one-electron.
- (v) Although their limitations must be recognized, DFT calculations provide useful qualitative insights into the leading superconfiguration description of the electronic structure of the lanthanide oxides.

### 3. Ce MOLECULES

Cerium materials beyond the oxides have fascinating properties. For example, cerium hexaboride, a hard ceramic used as an electron gun cathode material, is a heavy fermion material and possesses hidden magnetic phases. He bulk lattice, the boron atoms constitute hexaboride octahedra and form a CsCl crystal structure with the  $\mathrm{Ce^{3+}}$  (4f6s°) centers. Of course, on surfaces, edges, and corners it is unlikely that the  $\mathrm{B_6}$  units would remain octahedral. Furthermore,  $\mathrm{CeB_6}$  oxidizes under typical operating conditions. To determine how the electronic structures of molecular models of edge or corner sites evolved from the boride to the oxoboryl to the boronyl to the oxide, we considered the PE spectra of  $\mathrm{CeB_6}^{-1.6}$   $\mathrm{CeB_3O_2}^{-1.5}$ ,  $\mathrm{Ce(BO)_2}^{-1.5}$  and  $\mathrm{CeO_2}^{-1.4}$ 

The spectra, molecular structures consistent with the spectra, and natural ionization orbitals (NIOs) associated

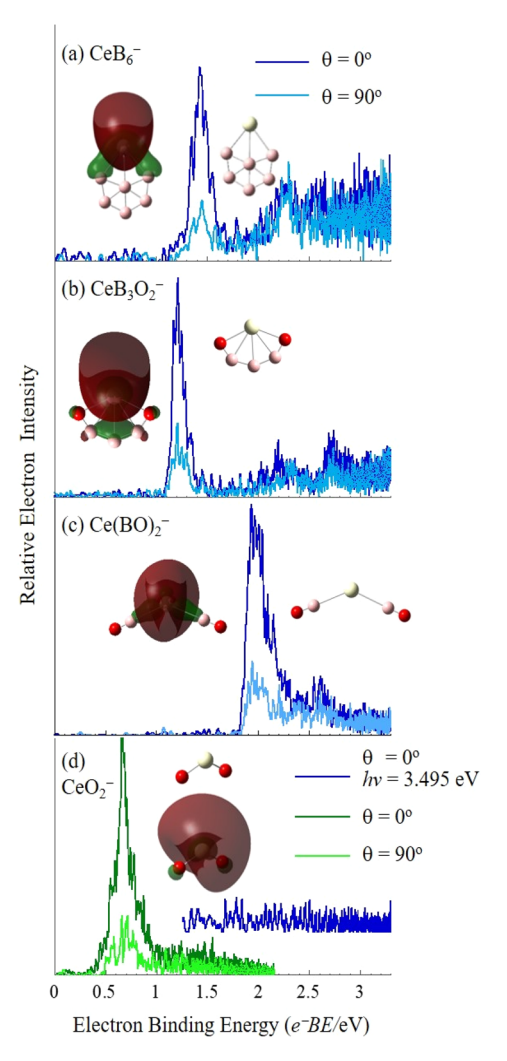


**Figure 3.** PE spectra and detachment NIOs of (a)  $CeB_6^-$ , (b)  $Ce(B_3O_2)^-$ , (c)  $Ce(BO)_2^-$ , and (d)  $CeO_2^-$ . Dark traces indicate laser polarization parallel to the electron drift path, and lighter traces indicate perpendicular polarization. The dominant features are more intense in the parallel polarization spectra, supporting the 6s-like NIOs shown. The features at higher electron binding energy in (a) and (b) are more isotropic, consistent with detachment from the boride or oxoboryl ligand. Blue and green traces indicate photon energies of 3.495 and 2.330 eV, respectively.

with the lowest-energy transitions in each spectrum are shown in Figure 3. NIOs provide a compact orbital-based illustration of the one-electron orbital where the change in charge occurs in the transition from the anion to the neutral. In Koopmans electron detachment processes, the NIO model is rigorously equivalent to the Dyson orbital model. In other situations, NIOs appear essentially equivalent to Dyson orbitals derived from high-order propagator methods. However, the formal relationship between NIOs and Dyson orbitals under such conditions remains an area of active research.

In all four molecular anions, the NIO is a diffuse 6s-like orbital, as with the diatomics. These molecules are ionic: the  $CeB_6^-$  anion can be described as  $Ce^{2+}(4f6s)B_6^{3-}$ , with the most intense feature observed in the spectrum (Figure 2a) associated with a transition to  $Ce^{3+}(4f)B_6^{3-}$ , while detachments of electrons from the  $B_6$  ligand appear as broad features with isotropic photoelectron angular distribution (PAD) to higher electron binding energy. Particularly interesting is the

neutral molecule, which adapts the same ionic character as the bulk, though the  $B_6$  ligand is clearly less compact than the octahedral structures in the bulk material, relaxing to a planar or nearly planar structure to accommodate the high negative charge. The teardroplike structure of  ${\rm CeB_6}^-/{\rm CeB_6}$  is similar to the structure inferred from the anion PE spectrum of  ${\rm SmB_6}^-$  reported previously. Wang and co-workers have undertaken extensive studies of metal borides,  $^{48-53}$  which largely feature planar or near-planar boride cluster ligands.  $^{47,49,51}$ 

Oxidation of CeB<sub>6</sub> surfaces is believed to play a role in the electron emission properties, and the electronic structures of the oxoboryl, boronyl, and oxide complexes give some insight into why. Similar to CeB<sub>6</sub><sup>-</sup>, CeB<sub>3</sub>O<sub>2</sub><sup>-</sup> can be described as  $Ce^{2+}(4f6s)[B_3O_2]^{3-}$ . As shown schematically in Figure 4, both  $CeB_6^-$  and  $CeB_3O_2^-$  have molecular orbitals crowded between

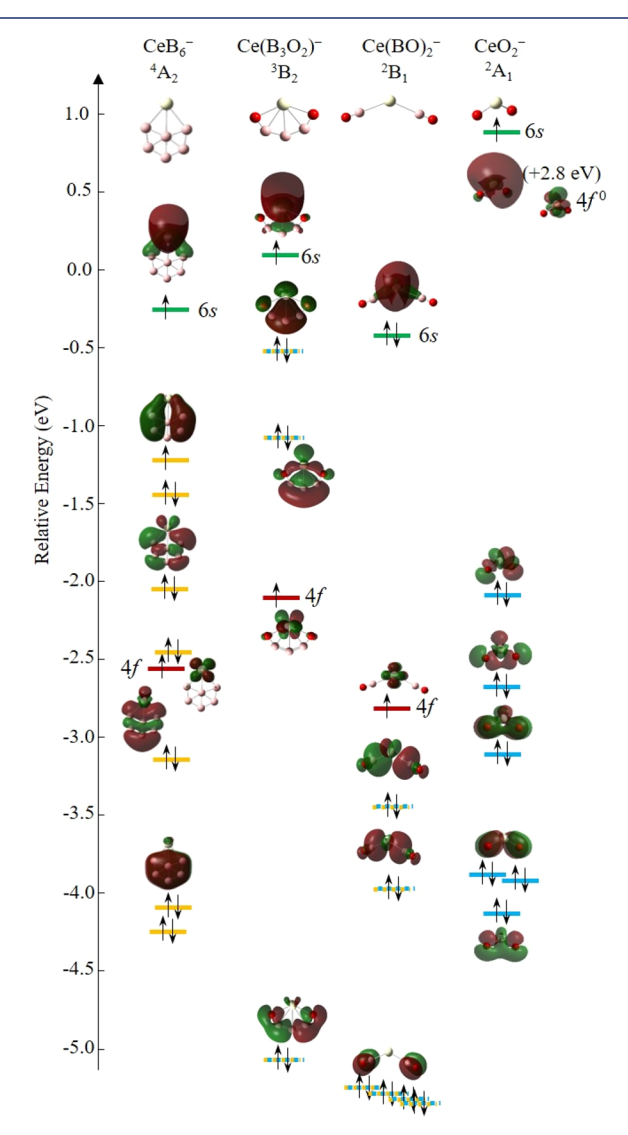


**Figure 4.** Schematic of the relative molecular orbital energies and occupancies of  $CeB_6^-$ ,  $Ce(B_3O_2)^-$ ,  $Ce(BO)_2^-$ , and  $CeO_2^-$ , showing the presence of boride or oxoboryl-local orbitals just below the diffuse Ce 6s orbital and core-like 4f orbital. In other molecular systems described in this report (e.g.,  $LnO^-$ ,  $Ce(BO)_2^-$ , larger metal oxide clusters), there is a significant energy gap between the 4f an 6s-like orbitals. B 2p-based MOs are indicated in orange, O 2p-based MOs in blue, Ce 6s-based in green and 4f-based in red. Mixed B/O 2p-based are indicated by blue and orange striped bars.

the Ce 4f and 6s orbitals. However, in the case of  $CeB_3O_2^-$ , the HOMO-1 localized on the oxoboryl ligand is particularly close in energy to the 6s singly occupied MO (neutral LUMO). Under the assumption that the diffuse 6s orbital plays a role in the thermal emission of the lanthanide borides, an occupied orbital lying energetically just below the 6s orbital would enhance the thermal emission. However, it should also be noted that this effect is reversed in the more oxidized  $Ce(BO)_2^-$  and  $CeO_2^-$  molecules.

This study gives insight into how the  $B_6^{3-}$  ligands may relax and oxidize at the surface and shows that with or without partial oxidation, the frontier orbitals are very close in energy to a diffuse 6s-like orbital (which would form a delocalized band on the surface). A recurring theme in these spectra is the fairly modest binding energy of electrons in this diffuse orbital, which by extension to the bulk facilitates electron emission from the surface.

This series of molecules provides another interesting insight.  $Ce(BO)_2^-$  features the Ce center with the  $CeO^-$ -like  $4f6s^2$  superconfiguration, while the Ce center in  $CeO_2^-$  has the  $4f^06s$  superconfiguration. Why is the 4f orbital in the anion not occupied, given the 6s orbital is higher lying in all of the other species? This is a poignant example of how the stronger Ce-O ionic bonding afforded by the empty 4f subshell in combination with the stabilization of the polarized 6s orbital by the dipole of the neutral "core" of  $CeO_2$  yields the non-aufbau orbital occupancy. The same effect was predicted for a  $C_{2\nu}$   $Ce_2O_4^-$  anion. However,  $(CeO_2)_n^-$  clusters with n>2 favor structures with small dipoles, and the HOMO is the 4f local orbital. 14

# 4. MIXED Ce-Sm OXIDE CLUSTERS

Because bonding in metal oxides is localized, cluster models provide a powerful platform for probing the properties of lowabundance bulk features such as corners, O vacancies, and dopants. 54,55 Interested in the possibility that O2- mobility in ceria may play a role in ceria support enhancement of catalyst performance and noting that Sm doping in ceria enhances the ionic conductivity, <sup>56-59</sup> we carried out studies of mixed Ce– Sm oxide clusters. <sup>12,18</sup> Samplings of PE spectra obtained at photon energies of 2.330 eV (green) and 3.495 eV (blue) for  $Ce_{3-x}Sm_xO_4^-$  and  $Ce_{3-x}Sm_xO_3^-$  (x = 0-3) are shown in Figures 5 and 6, respectively. As with the other species described above, the transitions to the ground states of all neutrals (X) exhibit parallel photoelectron angular distributions. Figure 5 shows the spectra of the Ce<sub>3-x</sub>Sm<sub>x</sub>O<sub>4</sub><sup>-</sup> series, all of which exhibit nearly identical spectral signatures of detachment of a fairly weakly bound electron from a nonbonding orbital with a much less intense shake-up lying ca. 0.5 eV higher in energy. While not shown here, the HOMOs of these anions can be described as linear combinations of the diffuse Ln 6s orbitals. The similarity of these spectra illustrates the chemical similarity noted above, with the incremental increase in the occupancy of the corelike 4f subshell with Z having a small impact on valence bonding. Since these tetroxide species have the simplest electronic structures of the various  $Ce_{3-x}Sm_xO_v^-$  (y = 3, 4) clusters, we discuss their electronic structures first.

Our earlier studies of  $\mathrm{Ce_xO_y}^-$  clusters  $^9$  suggested interesting parallels between the cluster and bulk electronic structures.  $^{60-64}$  For example, as with bulk  $\mathrm{Ce_2O_3}$ , the singly occupied 4f orbitals in the small  $\mathrm{Ce_xO_y}$  anion and neutral clusters lie energetically several electronvolts above the O-2p-

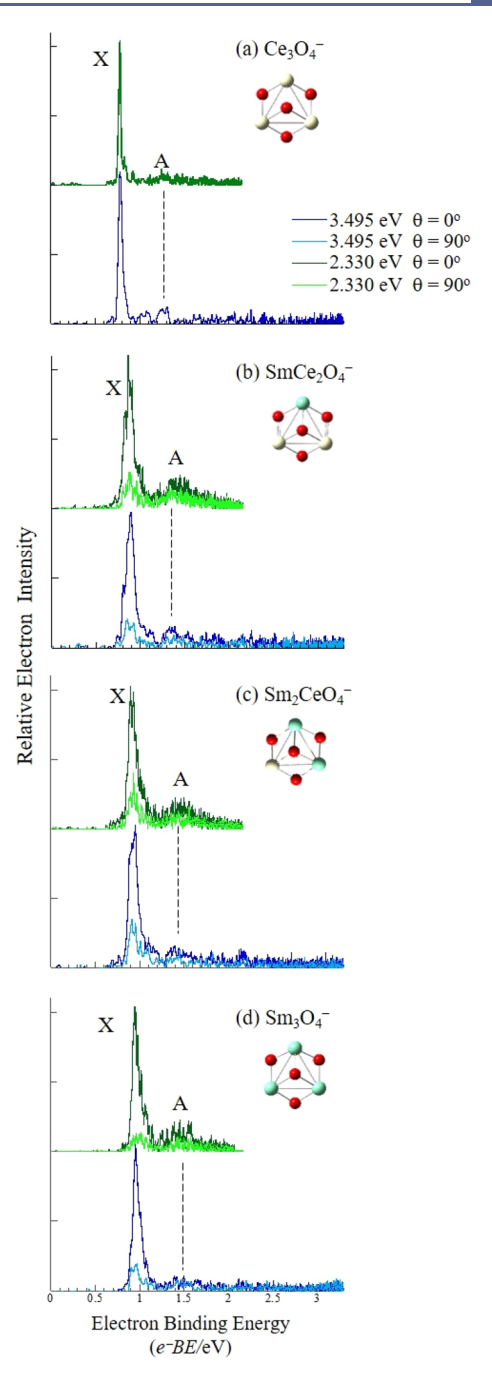


**Figure 5.** PE spectra and molecular structures of  $Ce_{3-x}Sm_xO_4^-$  (x=0-3) clusters, showing close similarity in electronic structures across the series, including the low-intensity features attributed to shake-up transitions. The slight broadening of the transitions with increasing x reflects the higher density of states in the 4f subshell occupancy in Sm versus 4f in Ce.

predominant orbitals, correlating to the bulk valence band. Additional electrons beyond those occupying the 2p or 4f orbitals lie in delocalized orbitals, evocative of the conduction band, that lie several electronvolts above the 4f orbitals. Figure 7 shows the relative occupied orbital energies schematically. Similarly, our studies of  $\mathrm{Sm}_x\mathrm{O}_y^-$  clusters suggest that the 4f band lies energetically with the highest-energy O 2p molecular orbitals and exhibits some 4f–2p covalency, as is the case with bulk  $\mathrm{Sm}_2\mathrm{O}_3$ . Included in Figure 7 are the molecular structures of  $\mathrm{Ce}_3\mathrm{O}_4^-$  and  $\mathrm{Sm}_3\mathrm{O}_4^-$  and the two

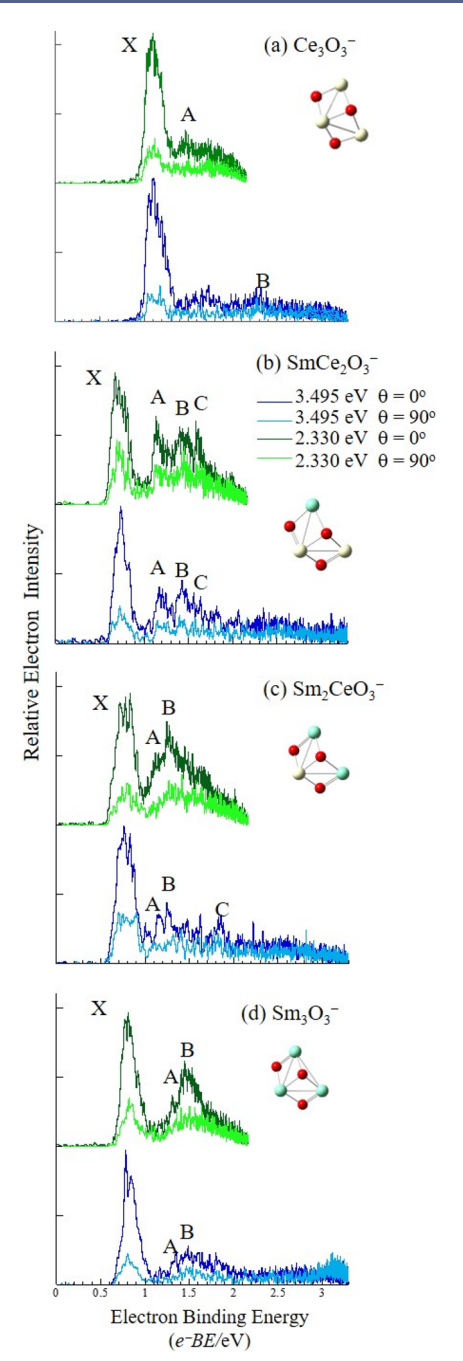


**Figure 6.** PE spectra and molecular structures of  $Ce_{3-x}Sm_xO_3^-$  (x=0-3) clusters, which contrast with those of the  $Ce_{3-x}Sm_xO_4^-$  (x=0-3) series in that the species with  $x \neq 0$  have a distinctly lower electron binding energy (position of band X) and more pronounced excited-state transitions (A, B, and C) than the pure  $Ce_3O_3^-$  cluster. In addition, these excited-state transitions are significantly more intense relative to X in the spectra measured with a photon energy of 2.330 eV compared with the spectra measured with a photon energy of 3.495 eV.

mixed species determined from our studies, along with the calculated orbital energies. All of the orbitals lying above the gray boxes, which represent the energy range of the fully occupied O-2p-predominant orbitals (correlating to the valence band of bulk  $Ln_2O_3$ ), are singly occupied, so species with Sm centers assume very high spin states or antiferromagnetically coupled spin states. While these calculated orbital

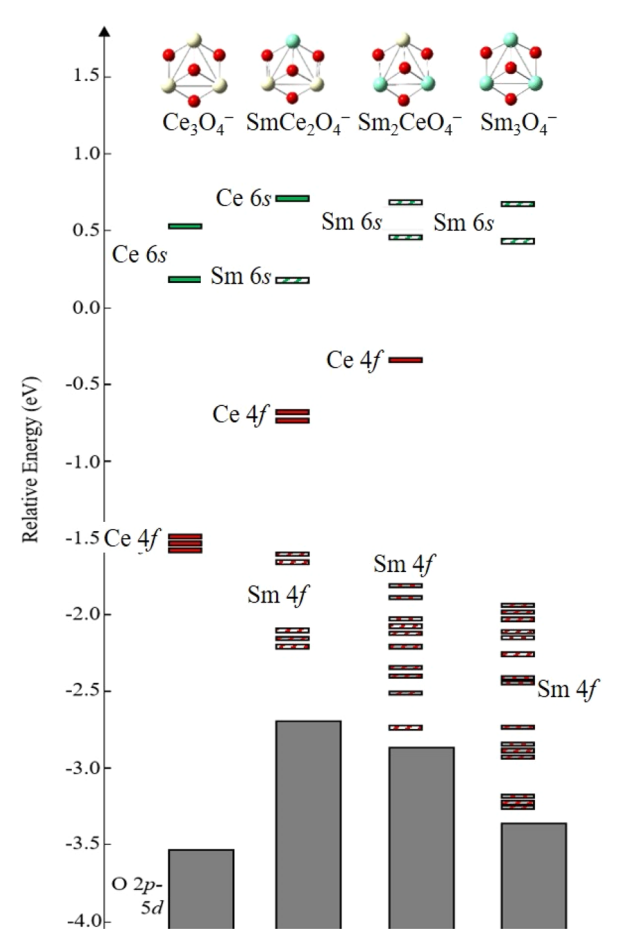


**Figure 7.** Schematic of the relative energies of singly occupied molecular orbitals for  $\mathrm{Sm}_x\mathrm{Ce}_{3-x}\mathrm{O_4}^-$  (x=0-3) along with the fully occupied O 2p-Ln Sd-based bonding MOs (gray), showing the incremental destabilization of the Ce 4f orbitals and the bulklike crowding of the Sm 4f "band" near the bonding orbitals with increasing x. Solid-filled shapes indicate Ce-based MOs, and hatchfilled shapes indicate Sm based MOs. The characters of the orbitals are indicated by the colors green, red, and gray for 6s, 4f, and 2p-5d, respectively.

energies do not align perfectly with the bulk band structure, from a qualitative standpoint the parallels are evident.

An interesting distinction between the  $Ln_x O_y$  anion and neutral clusters and the bulk is that the bulk conduction band has predominantly Ln 5d character. In small clusters, the 6s orbitals are stabilized relative to the 5d orbitals, and the HOMOs of these systems can be described as delocalized orbitals that envelope the cluster. The inference is that the 6s band is destabilized in the bulk because the interatomic distances are confining to these diffuse orbitals, BUT on edges, corners, and O vacancies on the surface, the 6s orbitals lie below the conventional conduction band.

For a number of  $\mathrm{Sm_xO_y}^-$  clusters or mixed Ce–Sm oxides with average metal oxidation states lower than +3, an interesting effect was observed in the PE spectra. As can be seen in the spectra of  $\mathrm{Ce_{3-x}Sm_xO_3}^-$  (x=1-3) shown in Figure 6b–d, the intensities of transitions to excited states (A, B, ...) relative to X are higher in the spectra measured with 2.330 eV photons than with 3.495 eV photons. The PE spectrum of  $\mathrm{Ce_3O_3}^-$  does not share this effect. While increases in the transition intensity with photon energy are observed when the detachment energy is resonant with transitions to excited anion

states embedded in the detachment continuum, it seemed unlikely that a wide range of Sm and mixed Ce—Sm oxides happened to coincidentally have excited anion states lying 2.330 eV above their anion ground states.

The simplest system that exhibited this effect was Sm<sub>2</sub>O<sup>-,12</sup> and the PE spectrum of Sm<sub>2</sub>O<sup>-</sup> was subsequently measured over a range of photon energies, as shown in Figure 8. The

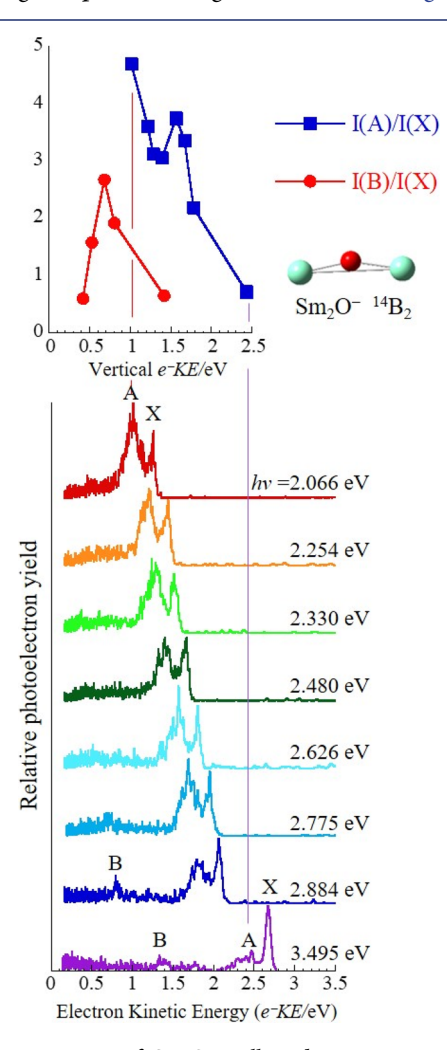


**Figure 8.** PE spectra of  $Sm_2O^-$  collected over a range of photon energies, along with a plot of the populations of excited states corresponding to bands "A" and "B" relative to "X" as functions of the vertical electron kinetic energy.

spectra are plotted as a function of electron kinetic energy (e<sup>-</sup>KE) to illustrate that there are not particular electron kinetic energies that are enhanced, as would be the likely if autodetachment of a quasibound anion state were the root cause: in general, autodetachment of a quasi-bound anion is coupled with vibrational relaxation of the neutral core, which imparts a unique quantum of electron kinetic energy.

What does this series of spectra shown in Figure 8 tell us? As the detachment energy is reduced, and the overall e<sup>-</sup>KE is reduced, the probability of populated excited neutral states relative to the ground neutral state is increased. The very high density of electronic states observed in these Sm-rich clusters in low oxidation states is quite unique. Consider the simple diatomic SmO (vide supra): the more reduced triatomic Sm<sub>2</sub>O would have more than double the number of states of SmO. We therefore proposed a theoretical platform that rejects the

typical treatment of photodetachment as an instantaneous process. Instead, a time-dependent treatment was employed wherein the final neutral state is derived from the superposition of densely packed neutral states interacting with the photoelectron and evolving in time. Slower electrons interact with the neutral for a longer time, resulting in a more pronounced effect.<sup>20</sup> This treatment predicted that the final excited-state population is inversely proportional to the electron momentum, i.e., proportional to the amount of time the electron resides in the range in which electron-neutral interactions are strong, which tracks well with the general shape of the ratio of the intensity of band A to the intensity of band X, which is shown in the top panel of Figure 8. However, we believe that the oscillation in the experimental relative intensity is due to 6s → 5d or some other electronic excitation in the anion. This effect is an ongoing line of research in our laboratory.

### 5. CONCLUDING REMARKS

The conclusion we draw from the strong electron-neutral interactions suggested in the PE spectra of the mixed Sm-Ce oxide cluster anions is that future models should assume that the one-electron picture of anion PE spectroscopy is inappropriate for molecules with exceptionally complex electronic structures and high densities of accessible neutral states. The molecule with the simplest electronic structure presented here, CeO, is still complicated in that it has 16 electronic states sharing a common superconfiguration within the energy range of several vibrational levels, with numerous additional low-lying states associated with the close-lying unoccupied 5d orbitals. In the case of Sm<sub>2</sub>O<sup>-</sup> and  $Ce_{3-x}Sm_xO_3^-$  (x = 1-3) clusters, the dramatic increase in the intensity of very low lying excitations with decreasing electron momentum invokes a picture in which a photoelectron induces electronic rearrangement in the neutral as it departs.

There are a number of unanswered questions, such as the following: (1) What exactly is the nature of the excitations that are enhanced by strong electron—neutral interactions? (2) Can the effect be tuned with Ln identity toward the center of the lanthanide row and are there other Ln-Ln' combinations that would produce a more dramatic effect? (3) What can be learned from the resonances in the I(A)/I(X) ratio? (4) What is the lifetime of these excited states?

Future theoretical work will involve enhancements to spin projection models for handling the multitude of available spin configurations in mixed lanthanide oxide clusters as well as the incorporation of such theories with models treating relativistic effects, particularly spin—orbit effects. The work described here has also inspired new theory based on the NIO model. Among new directions is the use of NIOs as a basis for (real-time) time-dependent simulations exploring relaxation of the electron density in response to electron detachment. Such a model will be used to explore strong electron—neutral cluster interactions, which will clearly have broader implications.

#### AUTHOR INFORMATION

# **Corresponding Authors**

\*E-mail: cjarrold@indiana.edu. \*E-mail: hhrachian@ucmerced.edu.

ORCID

Hrant P. Hratchian: 0000-0003-1436-5257 Caroline Chick Jarrold: 0000-0001-9725-4581 Accounts of Chemical Research

#### **Author Contributions**

The manuscript was written through contributions of all authors. All of the authors approved the final version of the manuscript.

#### **Funding**

NSF Grant CHE-1265991 and DOE Grant DE-FG02-07ER15889 (C.C.J.); ACS-PRF Grant 56806-DNI6, the Hellman Fellows Fund, and NSF CHE-1848580 (H.P.H.); IU-MSI STEM Initiative, with funding from Department of Navy Grant N000141512423.

#### **Notes**

The authors declare no competing financial interest.

#### **Biographies**

**Jarrett L. Mason** is a graduate student at IU. His research focuses on exploring the electronic structure of catalytically relevant metal oxides and lanthanide-based materials. He obtained his B.S. in chemistry from Birmingham-Southern College.

Hassan Harb is a Ph.D. candidate at UC Merced. He obtained his B.S. in chemistry at Lebanese American University and his M.S. in inorganic chemistry at American University of Beirut. His current research includes the modeling of photodetachment processes from lanthanide oxide and boride clusters.

Josey E. Topolski completed her B.S. and undergraduate research at the University of Rochester in 2014 and earned her Ph.D. at IU in 2018. Currently she is a senior scientist in the Analytical Sciences Division at Merck working on the preclinical development of pharmaceutical products.

Hrant P. Hratchian, a Michigan native, earned his B.S. at Eastern Michigan University and did graduate studies at Wayne State University. After postdoctoral training at IU, he began his independent career as a Research Scientist at Gaussian, Inc., in 2008. Since 2013 he has been Assistant Professor of Chemistry at UC Merced. His research program is focused on the theoretical and computational study of chemical systems involving transition metal (and inner-transition metal) elements.

Caroline Chick Jarrold, also a Michigan native, did her graduate studies at UC Berkeley. Following postdoctoral research at UCLA, she was appointed to the faculty at the University of Illinois at Chicago in 1997. She has been at Indiana University since 2002, where she is now Herman B. Wells Professor and Chemistry Department Chair.

# REFERENCES

- (1) Kramida, A.; Ralchenko, Yu.; Reader, J.; NIST ASD Team. *NIST Atomic Spectra Database*, version 5.6.1; National Institute of Standards and Technology: Gaithersburg, MD, 2018; https://physics.nist.gov/asd (accessed April 2, 2019).
- (2) van der Kolk, E.; Dorenbos, P. Systematic and Material Independent Variation of Electrical, Optical, and Chemical Properties of Ln Materials over the Ln Series (Ln = La, Ce, Pr, ..., Lu). *Chem. Mater.* **2006**, *18*, 3458–3462.
- (3) Allegre, C. J.; Poirier, J.-P.; Humler, E.; Hofmann, A. W. The Chemical-Composition of the Earth. *Earth Planet. Sci. Lett.* **1995**, *134*, 515–516.
- (4) Bruix, A.; Rodriguez, J. A.; Ramirez, P. J.; Senanayake, S. D.; Evans, J.; Park, J. B.; Stacchiola, D.; Liu, P.; Hrbek, J.; Illas, F. A New Type of Strong Metal—Support Interaction and the Production of H<sub>2</sub> through the Transformation of Water on Pt/CeO<sub>2</sub>(111) and Pt/CeO<sub>x</sub>/TiO<sub>2</sub>(110) Catalysts. *J. Am. Chem. Soc.* **2012**, *134*, 8968–8974.
- (5) Meunier, F. C.; Tibiletti, D.; Goguet, A.; Reid, D.; Burch, R. On the Reactivity of Carbonate Species on a Pt/CeO<sub>2</sub> Catalyst under

Various Reaction Atmospheres: Application of the Isotopic Exchange Technique. *Appl. Catal., A* **2005**, 289, 104–112.

Article

- (6) Felton, J. A.; Ray, M.; Waller, S. E.; Kafader, J. O.; Jarrold, C. C.  $Ce_xO_y^-$  (x=2-3) +  $D_2O$  Reactions: Stoichiometric Cluster Formation from Deuteroxide Decomposition and Anti-Arrhenius Behavior. *J. Phys. Chem. A* **2014**, *118*, 9960–9969.
- (7) Topolski, J. E.; Kafader, J. O.; Ray, M.; Jarrold, C. C. Elucidating Cerium + H<sub>2</sub>O Reactivity Through Electronic Structure: A Combined PES and DFT Study. *J. Mol. Spectrosc.* **2017**, 336, 1–11.
- (8) Aubriet, F.; Gaumet, J.-J.; deJong, W. A.; Groenewold, G. S.; Gianotto, A. K.; McIlwain, M. E.; Van Stipdonk, M. J.; Leavitt, C. M. Cerium Oxyhydroxide Clusters: Formation, Structure, and Reactivity. *J. Phys. Chem. A* **2009**, *113*, 6239–6252.
- (9) Kafader, J. O.; Topolski, J. E.; Jarrold, C. C. Molecular and Electronic Structures of Cerium and Cerium Suboxide Clusters. *J. Chem. Phys.* **2016**, *145*, 154306.
- (10) Ray, M.; Felton, J. A.; Kafader, J. O.; Topolski, J. E.; Jarrold, C. C. Photoelectron spectra of CeO<sup>-</sup> and Ce(OH)<sub>2</sub><sup>-</sup>. *J. Chem. Phys.* **2015**, *142*, 064305.
- (11) Kafader, J. O.; Ray, M.; Jarrold, C. C. Photoelectron Spectrum of PrO<sup>-</sup>. *J. Chem. Phys.* **2015**, *143*, 064305.
- (12) Kafader, J. O.; Topolski, J. E.; Marrero-Colon, V.; Iyengar, S. S.; Jarrold, C. C. The Electron Shuffle: Cerium Influences Samarium 4f Orbital Occupancy in Heteronuclear Ce—Sm Oxide Clusters. *J. Chem. Phys.* **2017**, *146*, 194310.
- (13) Kafader, J. O.; Ray, M.; Jarrold, C. C. Low-lying Electronic Structure of EuH, EuOH, and EuO Neutrals and Anions Determined by Anion Photoelectron Spectroscopy and DFT Calculations. *J. Chem. Phys.* **2015**, *143*, 034305.
- (14) Topolski, J. E.; Kafader, J. O.; Jarrold, C. C. Ce in the +4 Oxidation State: Anion Photoelectron Spectroscopy and Photodissociation of Small Ce<sub>x</sub>O<sub>y</sub>H<sub>z</sub><sup>-</sup> Molecules. *J. Chem. Phys.* **2017**, *147*, 104303.
- (15) Mason, J. L.; Harb, H.; Topolski, J. E.; Hratchian, H. P.; Jarrold, C. C. A Tale of Two Stabilities: How One Boron Atom Affects a Switch in Bonding Motifs in  $CeO_2B_x^-$  (x=2,3) Complexes. *J. Phys. Chem. A* **2018**, 122, 9879–9885.
- (16) Mason, J. L.; Harb, H.; Huizenga, C. D.; Ewigleben, J. C.; Topolski, J. E.; Hratchian, H. P.; Jarrold, C. C. Electronic and Molecular Structures of the CeB<sub>6</sub> Monomer. *J. Phys. Chem. A* **2019**, 123, 2040–2048.
- (17) Ray, M.; Kafader, J. O.; Topolski, J. E.; Jarrold, C. C. Mixed Cerium—Platinum Oxides: Electronic Structure of [CeO]Pt<sub>n</sub> (n=1, 2) and [CeO<sub>2</sub>]Pt complex anions and neutrals. *J. Chem. Phys.* **2016**, 145, 044317.
- (18) Topolski, J. E.; Kafader, J. O.; Marrero-Colon, V.; Iyengar, S. S.; Hratchian, H. P.; Jarrold, C. C. Exotic Electronic Structures of  $\mathrm{Sm}_x\mathrm{Ce}_{3-x}\mathrm{O}_y$  ( $x=0-3;\ y=2-4$ ) Clusters and the Effect of High Neutral Density of Low-lying States on Photodetachment Transition Intensities. *J. Chem. Phys.* **2018**, *149*, 054305.
- (19) Wigner, E. P. On the Behavior of Cross Sections Near Thresholds. *Phys. Rev.* **1948**, *73*, 1002–1009.
- (20) Mason, J. L.; Topolski, J. E.; Ewigleben, J. C.; Iyengar, S. S.; Jarrold, C. C. Photoelectrons Are Not Always Quite Free. *J. Phys. Chem. Lett.* **2019**, *10*, 144–149.
- (21) Field, R. W. Diatomic Molecule Electronic Structure beyond Simple Molecular Constants. *Ber. Bunsen-Ges. Phys. Chem.* **1982**, *86*, 771–779.
- (22) Kaledin, L. A.; McCord, J. E.; Heaven, M. C. Laser Spectroscopy of CeO: Characterization and Assignment of States in the 0–3 eV Range. *J. Mol. Spectrosc.* **1993**, *158*, 40–61.
- (23) Kaledin, L. A.; McCord, J. E.; Heaven, M. C. Rotation—Electronic Deperturbation Analysis of the 4f 6s Configurational States of CeO. J. Mol. Spectrosc. 1995, 170, 166–171.
- (24) Linton, C.; Chen, J.; Steimle, T. C. Permanent Electric Dipole Moment of Cerium Monoxide. *J. Phys. Chem. A* **2009**, *113*, 13379–13382.
- (25) Linton, C.; Dulick, M.; Field, R. W.; Carette, P.; Leyland, P. C.; Barrow, R. F. Electronic states of the CeO molecule: Absorption,

emission, and laser spectroscopy. J. Mol. Spectrosc. 1983, 102, 441–497.

- (26) Dolg, M.; Stoll, H.; Preuss, H. The Low-lying Electronic States of Cerium Monoxide CeO- Ab initio Calculations Using Energy-Adjusted Pseudopotentials and Spin-orbit Operators. *J. Mol. Struct.:* THEOCHEM 1991, 231, 243–255.
- (27) Todorova, T. K.; Infante, I.; Gagliardi, L.; Dyke, J. M. The Chemiionization Reactions Ce + O and Ce +  $O_2$ : Assignment of the Observed Chemielectron Bands. *Int. J. Quantum Chem.* **2009**, 109, 2068–2079.
- (28) Zhang, Q.; Hu, S.-X.; Qu, H.; Su, J.; Wang, G.; Lu, J. B.; Chen, M.; Zhou, M.; Li, J. Pentavalent Lanthanide Compounds: Formation and Characterization of Praseodymium(V) Oxides. *Angew. Chem., Int. Ed.* **2016**, *55*, 6896–6900.
- (29) Hu, S.-X.; Jian, J.; Su, J.; Wu, X.; Li, J.; Zhou, M. Pentavalent Lanthanid Nitride-Oxides: NPrO and NPrO<sup>−</sup> Complexes with N≡Pr Triple Bonds. *Chem. Sci.* **2017**, *8*, 4035–4043.
- (30) Felton, J. A.; Ray, M.; Jarrold, C. C. Measurement of the Electron Affinity of Atomic Ce. *Phys. Rev. A: At., Mol., Opt. Phys.* **2014**, 89, 033407.
- (31) O'Malley, S. M.; Beck, D. R. Calculation of Ce<sup>-</sup> Binding Energies by Analysis of Photodetachment Partial Cross Sections. *Phys. Rev. A: At., Mol., Opt. Phys.* **2006**, *74*, 042509.
- (32) Weichman, M. L.; Vlaisavljevich, B.; DeVine, J. A.; Shuman, N. S.; Ard, S. G.; Shiozaki, T.; Neumark, D. M.; Viggiano, A. A. Electronic Structure of SmO and SmO<sup>-</sup> via Slow Photoelectron Velocity-Map Imaging Spectroscopy and Spin-Orbit CASPT2 Calculations. *J. Chem. Phys.* **2017**, *147*, 234311.
- (33) Waller, S. E.; Mann, J. E.; Jarrold, C. C. Asymmetric Partitioning of Metals among Cluster Anions and Cations Generated via Laser Ablation of Mixed Aluminum/Group 6 Transition Metal Targets. J. Phys. Chem. A 2013, 117, 1765–1772.
- (34) Moravec, V. D.; Jarrold, C. C. Study of the Low-lying States of NiO<sup>-</sup> and NiO Using Anion Photoelectron Spectroscopy. *J. Chem. Phys.* **1998**, *108*, 1804–1810.
- (35) Cooper, J.; Zare, R. N. Angular Distribution of Photoelectrons. J. Chem. Phys. 1968, 48, 942–943.
- (36) Reed, K. J.; Zimmerman, A. H.; Andersen, H. C.; Brauman, J. I. Cross sections for photodetachment of electrons from negative ions near threshold. *J. Chem. Phys.* **1976**, *64*, 1368–1375.
- (37) Moriyama, H.; Tatewaki, H.; Yamamoto, S. Electronic Structure of CeO studied by a Four-Component Relativistic Configuration Interaction Method. *J. Chem. Phys.* **2013**, *138*, 224310.
- (38) Klingeler, R.; Lüttgens, G.; Pontius, N.; Rochow, R.; Bechthold, P. S.; Neeb, M.; Eberhardt, W. Photoelectron Spectra of Small LaO<sub>n</sub><sup>-</sup> Clusters: Decreasing electron affinity upon increasing the number of oxygen atoms. *Eur. Phys. J. D* **1999**, *9*, 263–267.
- (39) Dulick, M.; Murad, E.; Barrow, R. F. Thermochemical Properties of the Rare Earth Monoxides. *J. Chem. Phys.* **1986**, *85*, 385–390.
- (40) Carette, P.; Hocquet, A. Ligand-Field Calculation of the Lower Electronic-Energy Levels of the Lanthanide Monoxides. *J. Mol. Spectrosc.* **1988**, *131*, 301–324.
- (41) Douglas, M.; Kroll, N. M. Quantum Electrodynamical Corrections to the Fine Atructure of Helium. *Ann. Phys.* **1974**, 82, 89–155.
- (42) Hess, B. A. Applicability of the No-Pair Equation with Free-Particle Projection Operators to Atomic and Molecular Structure Calculations. *Phys. Rev. A: At., Mol., Opt. Phys.* **1985**, 32, 756–763.
- (43) Hess, B. A. Relativistic Electronic-Structure Calculations Employing a Two-Ccomponent No-Pair Formalism with External-Field Projection Operators. *Phys. Rev. A: At., Mol., Opt. Phys.* **1986**, 33, 3742–3748.
- (44) Schell, G.; Winter, H.; Rietschel, H.; Gompf, F. Electronic Structure and Superconductivity in Metal Hexaborides. *Phys. Rev. B: Condens. Matter Mater. Phys.* **1982**, 25, 1589–1599.
- (45) Duan, J.; Zhou, T.; Zhang, L.; Du, J. G.; Jiang, G.; Wang, H. B. Elastic Properties and Electronic Structures of Lanthanide Hexaborides. *Chin. Phys. B* **2015**, *24*, No. 096201.

- (46) Thompson, L. M.; Harb, H.; Hratchian, H. P. Natural Ionization Orbitals for Interpreting Electron Detachment Processes. *J. Chem. Phys.* **2016**, *144*, 204117.
- (47) Robinson, P. F.; Zhang, X.; McQueen, T.; Bowen, K. H.; Alexandrova, A. N. SmB<sub>6</sub><sup>-</sup> Cluster Anion: Covalency Involving f Orbitals. *J. Phys. Chem. A* **2017**, *121*, 1849–1854.
- (48) Romanescu, C.; Sergeeva, A. P.; Li, W. L.; Boldyrev, A. I.; Wang, L.-S. Planarization of  $B_7^-$  and  $B_{12}^-$  Clusters by Isoelectronic Substitution:  $AlB_6^-$  and  $AlB_{11}^-$ . J. Am. Chem. Soc. **2011**, 133, 8646–8653.
- (49) Chen, T.-T.; Li, W.-L.; Chen, W. J.; Li, J.; Wang, L.-S.  $\rm La_3B_{14}^-$ : An Inverse Triple-Decker Lanthanid Boron Cluster. *Chem. Commun.* **2019**, *55*, 7864–78678.
- (50) Chen, T.-T.; Li, W.-L.; Jian, T.; Chen, X.; Li, J.; Wang, L.-S.  $PrB_7^-$ : A Praseodymium-Doped Boron Cluster with a  $Pr^{II}$  Center Coordinated by a Doubly Aromatic Planar  $\eta^7$  -B $_7^{3-}$  Ligand. *Angew. Chem., Int. Ed.* **2017**, *56*, 6916–6920.
- (51) Chen, X.; Chen, T.-T.; Li, W.-L.; Lu, J. B.; Zhao, L. J.; Jian, T.; Hu, H. S.; Wang, L.-S.; Li, J. Lanthanides with Unusually Low Oxidation States in the PrB<sub>3</sub><sup>-</sup> and PrB<sub>4</sub><sup>-</sup> Boride Clusters. *Inorg. Chem.* **2019**, 58, 411–418.
- (52) Chen, T.-T.; Li, W.-L.; Li, J.; Wang, L.-S.  $[La(\eta^x-B_x)La]^-$  (x = 7-9): A New Class of Inverse Sandwich Complexes. *Chem. Sci.* **2019**, 10, 2534–2542.
- (53) Li, W.-L.; Chen, T.-T.; Xing, D.-H.; Chen, X.; Li, J.; Wang, L.-S. Observation of Highly Stable and Symmetric Lanthanide Octa-boron Inverse Sandwich Complexes. *Proc. Natl. Acad. Sci. U. S. A.* **2018**, *115*, E6972—E6977.
- (54) Lang, S. M.; Bernhardt, T. M. Gas Phase Metal Cluster Model Systems for Heterogeneous Catalysis. *Phys. Chem. Chem. Phys.* **2012**, *14*, 9255–9269.
- (55) Mann, J. E.; Mayhall, N. J.; Jarrold, C. C. Properties of Metal Oxide Clusters in Non-traditional Oxidation States. *Chem. Phys. Lett.* **2012**, 525–526, 1–12.
- (56) Yahiro, H.; Eguchi, Y.; Eguchi, K.; Arai, H. Oxygen Ion Conductivity of the Ceria–Samarium Oxide System with Fluorite Structure. *J. Appl. Electrochem.* **1988**, *18*, 527–531.
- (57) Fergus, J. W. Electrolytes for Solid Oxide Fuel Cells. J. Power Sources 2006, 162, 30-40.
- (58) Kharton, V. V.; Marques, F. M. B.; Atkinson, A. Transport Properties of Solid Oxide Electrolyte Ceramics: A Brief Review. *Solid State Ionics* **2004**, *174*, 135–149.
- (59) Coduri, M.; Checchia, S.; Longhi, M.; Ceresoli, D.; Scavini, M. Rare Earth Doped Ceria: The Complex Connection Between Structure and Properties. *Front. Chem.* **2018**, *6*, 526.
- (60) Skorodumova, N. V.; Ahuja, R.; Simak, S. I.; Abrikosov, I. A.; Johansson, B.; Lundqvist, B. I. Electronic, Bonding, and Optical Properties of CeO<sub>2</sub> and Ce<sub>2</sub>O<sub>3</sub> from First Principles. *Phys. Rev. B: Condens. Matter Mater. Phys.* **2001**, *64*, 115108.
- (61) Hay, P. J.; Martin, R. L.; Uddin, J.; Scuseria, G. E. Theoretical Study of CeO<sub>2</sub> and Ce<sub>2</sub>O<sub>3</sub> Using a Screened Hybrid Density Functional. *J. Chem. Phys.* **2006**, *125*, 034712.
- (62) Brugnoli, L.; Ferrari, A. M.; Civalleri, B.; Pedone, A.; Menziani, M. C. Assessment of Density Functional Approximations for Highly Correlated Oxides: The Case of CeO<sub>2</sub> and Ce<sub>2</sub>O<sub>3</sub>. *J. Chem. Theory Comput.* **2018**, *14*, 4914–4927.
- (63) Gillen, R.; Clark, S. J.; Robertson, J. Nature of the Electronic Band Gap in Lanthanide Oxides. *Phys. Rev. B: Condens. Matter Mater. Phys.* **2013**, 87, 125116.
- (64) Jiang, H.; Rinke, P.; Scheffler, M. Electronic Properties of Lanthanide Oxides from the GW Perspective. *Phys. Rev. B: Condens. Matter Mater. Phys.* **2012**, *86*, 125115.